1

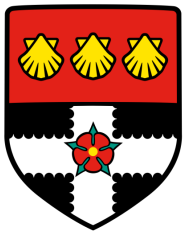

University of Reading

Department of Meteorology

To What Extent do Ocean Dynamics Affect Arctic Sea Ice Loss?

Nishit Jajodia

Supervisors: Jake Aylmer, David Ferreira

A report submitted in partial fulfilment of the requirements of
the University of Reading for the degree of
Master of Science in *Atmosphere, Ocean and Climate*

August 21, 2024

Declaration

I, Nishit Anand Jajodia, of the Department of Meteorology, University of Reading, confirm that this is my own work and figures, tables, equations, code snippets, artworks, and illustrations in this report are original and have not been taken from any other person's work, except where the works of others have been explicitly acknowledged, quoted, and referenced. I understand that failing to do so will be considered a case of plagiarism. Plagiarism is a form of academic misconduct and will be penalised accordingly.

I give consent to a copy of my report being shared with future students as an exemplar.

I give consent for my work to be made available more widely to members of UoR and the public with interest in teaching, learning and research.

Nishit Anand Jajodia

August 21, 2024

Abstract

Arctic sea ice has been in decline at an accelerated rate since the 1970s. The amount so sea ice cover in the Arctic is strongly driven by rise in global average surface air temperature and anthropogenic CO_2 emissions. There has been an increasing effort to understand the mechanisms by which heat it transported to and away from the Arctic and how it affects the sea ice levels and its distribution. But the relative roles of the atmosphere and ocean in driving changes remains uncertain. Though a strong correlation of sea ice extent with ocean heat transport (OHT) and atmospheric heat transport (AHT) has been established using both observations and model simulations, the direction of causation is not known. This is, in part, because of a large spread across models. Though most models agree that an increase in poleward OHT is positively correlated to a retreating Arctic ice-edge latitude (ϕ), it is not known which phenomenon is driving the change, or even if a causation exists at all. This study investigates this problem by looking at lead/lag correlations between changes in OHT, ϕ, AHT, average surface air temperatures (TAS) and the AMOC index for 4 CMIP6 models. We find that all models show a strong positive correlation between increasing TAS and retreating Arctic sea ice. All models also show a positive correlation between ΔOHT and $\Delta\phi$, with changes in OHT leading by 2-7 years, indicating that OHT might indeed be driving changes in sea ice and not the other way around. Some models also show an inversion of this correlation at higher latitudes. Along with the negative correlation between ΔAHT and $\Delta\phi$ at lower latitudes and positive at higher latitudes, we propose a mechanism where OHT remains the primary carrier of heat to the Arctic south of the ice edge location. At the edge, the heat it transported to the atmosphere which then distributes it over central Arctic. We also see that though the AMOC has a strong positive correlation with sea ice retreat, its relationship with OHT is uncertain due to large inter-model spread. Thus the mechanism by which the AMOC is related to Arctic sea ice trends remains uncertain.

Keywords: Arctic, sea ice, ocean heat transport, AMOC, CMIP6

Acknowledgements

I would like to thank Dr. Jake Aylmer and Dr. David Ferreira for their help with everything. Special thanks to Lei and Miriam for there constant support and motivation throughout this journey. I could not have asked for better friends. I would also like to mention Balaji and Jeric for always being there for me.

Contents

List of Figures

List of Tables

Chapter 1

Introduction

1.1 Arctic sea ice decline

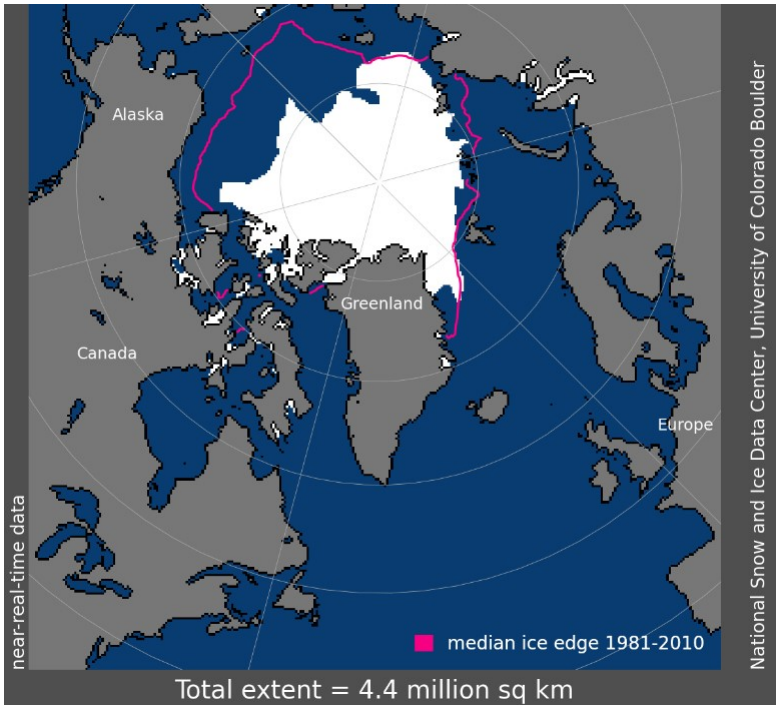

Figure 1.1: Median Arctic sea ice edge (pink line) in comparison to near real-time sea ice in September 2023. *Source: (Fetterer et al., 2017)*

The Arctic region (60°N- 90°N) is a mostly landless ocean, which is always partially covered by ice (Figure 1.1). Satellite observations have shown that Arctic sea ice has been thinning and retreating since the 1970s (Comiso et al., 2008, Serreze and Meier, 2019). The rate at which the sea ice is retreating is accelerating, going from about 0.25 million km^2/decade in

1980s to about 0.47 million km^2/decade in 2010s (Karami et al., 2023). In Figure 1.2, by NSIDC, University of Colorado, Boulder, we can see that the sea ice extent (SIE) in the Arctic has been decreasing since 1979. The fastest sea ice loss has been observed in western Arctic region (Liu et al., 2021, Docquier and Koenigk, 2021), with the Pacific North American (PNA) pattern driving 25% of the inter-annual variability (Liu et al., 2021). Arctic sea ice loss can lead to an increase in ocean heat uptake in sub-polar North Atlantic on smaller time scales and warming of lower to upper troposphere as well as other ocean basins on a multidecadal to centennial timescales (Li and Liu, 2022).

Since the year 2000, we have seen 4 record lows in September Arctic sea ice cover, with the lowest being in 2012 (Figure 1.2). Each of these events were lead by summers with abrupt low sea-level pressures, cloudiness and a split jet stream over East Asia, Scandinavia and northern North America (Francis and Wu, 2020). Both sea ice area (SIA) and sea ice volume (SIV) have been decreasing steadily since the 1970s. Docquier and Koenigk (2021) used observation and reanalysis data to calculate that between 1979 and 2000, the annual mean Arctic SIA has decreased by 18% (2 million km^2) and annual the annual mean Arctic SIV by 49% (12000 km^2). The winter sea ice thickness in the Arctic has been observed to have reduced by 0.37m or 20% between February/March 2008 and February/March 2008 (Petty et al., 2020). The residence of time of sea ice has drastically decreased, with Arctic sea ice undergoing a regime shift- from thick and deformed to thin and more uniform, between 2005 and 2007 (Sumata et al., 2023).

The loss of sea ice has been shown to have a strong relationship with increase in anthropogenic CO_2 emissions and global surface temperature rise. Stroeve and Notz (2018) show, using observations and CMIP5 model simulations, that there is a strong linear relationship between pan-Arctic SIE and total anthropogenic CO_2 emissions across all months, with loss of 1 m^2 per ton of anthropogenic CO_2 in winter and 3 m^2 throughout summer. By extrapolating these trends, they predict that the Arctic will become seasonally ice free in the August-September period if another 800 $\pm$ 300 Gt of CO_2 is added to the atmosphere. Karami et al. (2023) predict that if rate of sea ice loss keeps accelerating at the current rate, sea ice-free Septembers may start occurring around 2060 . Our analysis of the correlation between sea ice and surface air temperature can be found in Section 3.1.

Since dark water absorbs more heat sun light than the much brighter sea ice, declining ice leads to more absorption of heat, which in turn results in faster melting of the ice. This

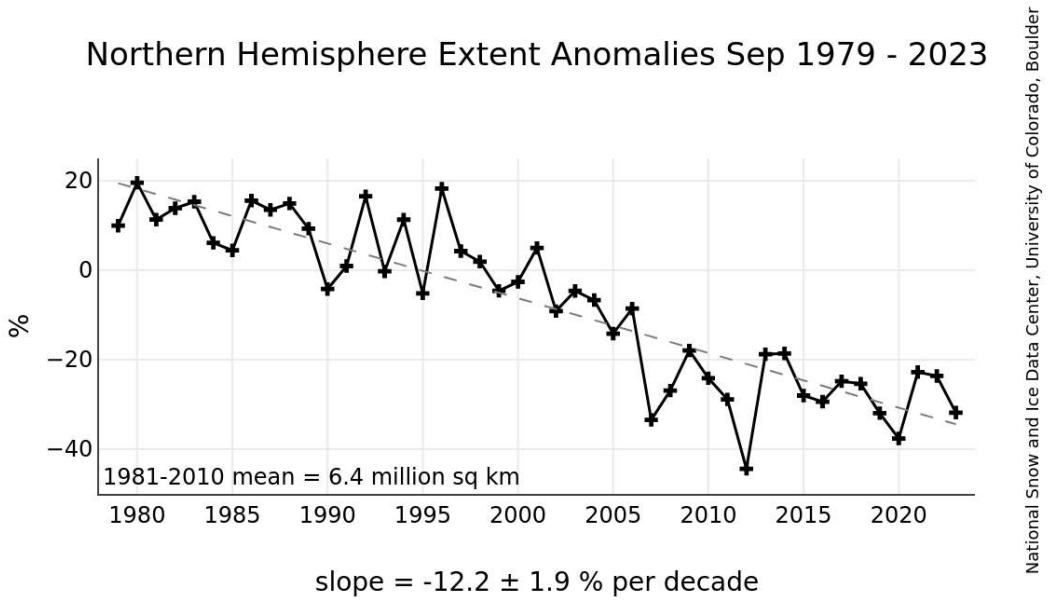

Figure 1.2: Annual mean Sea Ice Extent anomalies in the northern hemisphere, with respect to 1981-2010. Crosses and solid line represent the annual mean anomaly values and dashed line is the linear trend. *Source: (Fetterer et al., 2017)*

phenomenon is called Arctic Amplification and it has been suggested to have significant effects on energy balances (Johannessen et al., 2004).

The sensitivity of the Northern Hemisphere's near-surface atmosphere to sea ice loss has been shown to be robust during the cold season, as demonstrated by Hay et al. (2022) through sea ice-forced model simulations. However, the inter-model spread is larger during the boreal summer, indicating that the effects of sea ice loss on atmospheric conditions may vary more widely across different climate models during this season.

1.2 Impacts of Decline Arctic sea ice

The loss of Arctic sea ice cover has long term as well as short term effects on the Earth's climate system. The immediate local consequences of declining sea ice include increased turbulent heat fluxes—both sensible and latent—from the ocean to the atmosphere, along with an increase in long-wave radiation emitted by the sea surface, as discussed by Vihma (2014). They also note that this his has locally increased air temperature, moisture, and cloud cover and reduced the static stability in the lower troposphere.

Reduction in sea ice cover has also increased the sea surface area leading to increased

dissolved CO_2 concentrations in the ocean. Ouyang et al. (2020) show that between 1994 and 2017, summer time CO_2 concentration in the Canadian sea increased at twice the rate of atmospheric CO_2 increase in that region. This has lead to a decline in ocean-atmosphere CO_2 concentration gradient, which can have have significant impact on local marine ecosystems.

As the Arctic becomes seasonally ice free by the end of the 21st century, the ice loss will have increasingly larger effects on the Earth's climate system. Liu et al. (2022) predict that 37-48% of the increase in frequency of strong El Niño events by the end of this century will be a direct result of Arctic sea ice loss.

Changes in Arctic sea ice has major effects on large scale ocean circulation (Li and Liu, 2022). Reduction in sea ice results in the oceans absorbing more heat from the atmosphere, especially in the subpolar North Atlantic. Because of this the Atlantic Meridional Overturning Circulation (AMOC) does not change much since the heat is redistributed and stored locally in the Atlantic. But on multidecadal scales, as the AMOC weakens, the heat is distributed to other ocean basins resulting in large scale impacts (Li and Liu, 2022, Hay et al., 2022).

Therefore it is important to study the physical mechanisms driving changes in polar sea ice so that we better understand the implications of rapidly declining Arctic sea ice.

1.3 Drivers of Arctic Sea ice melting

An investigation using multidecadal-scale observational data in combination with ECHAM4 and HadCM3 coupled model simulation by Johannessen et al. (2004) revealed that the warming of the Arctic in 1920s-1930s, followed by cooling until 1970 was driven by natural internal climate variability. However warming of Arctic and loss of sea ice in subsequent decades could not be explained by natural processes and was driven by anthropogenic climate change driven near-surface air temperature change (Notz and Marotzke, 2012, Johannessen et al., 2004). Docquier et al. (2022) further emphasized the dominant role of near-surface air temperatures in driving recent and future changes in Arctic sea ice. Through an analysis of 50 ensemble members using the EC-Earth3 global climate model, covering the period from 1970 to 2100, they concluded that near-surface air temperatures and ocean heat transport (OHT) are the primary drivers of Arctic sea ice decline. While changes in sea ice themselves have feedback effects on both temperature and OHT, the influence of sea ice on these factors diminishes over time. Additionally, Cai et al. (2021) linked the long-term decline in Arctic sea ice from

1850 to 2017 to a combination of global warming and regional Arctic warming. These changes are influenced by several large-scale atmospheric oscillations, including the Arctic Oscillation, North Atlantic Oscillation, Atlantic Multidecadal Oscillation, and Pacific Decadal Oscillation. The phenomenon of Arctic Amplification, which enhances the positive ice/ocean albedo feedback loop has been suggested as a possible internal driver of rapid sea ice decline. variability explained (Johannessen et al., 2004). Cai et al. (2021) suggest that it plays significant role in accelerating summer sea ice decline. But the idea that Arctic amplification has dominated the accelerating long term sea ice decline in the recent decades was refuted by other studies like Notz and Marotzke (2012) and Stroeve and Notz (2018).

Seasonal and atmospheric circulation patterns also play a crucial role in modulating sea ice variability. For instance, Francis and Wu (2020) identified that the 4 summers since 2000 with record low September Arctic sea ice cover were all lead by August-September with an abrupt drop in mean sea level pressure (MSLP) and a split jet stream. This suggests that atmospheric dynamics, in conjunction with temperature increases, can exacerbate sea ice loss during certain periods. The spatially heterogeneous effect of Arctic cyclones has also been identified (Clancy et al., 2022), as decreasing sea ice to the east of the cyclones and increasing it to the west.

1.3.1 OHT as driver for Arctic Sea Ice

The influence of OHT on Arctic sea ice is not well understood due to greater inaccessibility of the ocean compared to the atmosphere. But there is an increasing effort to understand this crucial relationship, as well as the feedback mechanisms because of how the changes in the sea ice cover in turn change OHT.

An early study by Winton (2003) showed that SIE had a large sensitivity to the magnitude of ocean current. Stronger currents lead to reduced SIE and increased warming at high latitudes. They were also able to show that low cloudiness decreases with strengthening ocean circulations, leading to greater sea ice loss by reducing net reflectivity and warming the climate. Bitz et al. (2005) used a coupled global climate model to show that OHT that melts polar sea ice (at either pole) is driven primarily by the amount of solar radiation absorbed by the ocean and convergence of heat transported by different currents at the ice edge. At lower latitudes (in cases where sea ice-edge reaches low latitudes), the amount of solar radiation plays a larger role and at higher latitudes OHT convergence is more important. They also

showed that OHT convergence weakens near the ice-edges when the model is subject to increased CO_2 forcings.

A strong relationship between warming in the Atlantic Ocean and Arctic ocean has long been observed (Steele and Boyd, 1998, Polyakov et al., 2004, Schlichtholz, 2011). But recently there have been efforts to quantify the relationship between the heat transport in the Atlantic and Arctic sea ice (Docquier and Koenigk, 2021). Within the Arctic, the Barents Sea has been observed to show the maximum loss of sea ice as well as heat transport towards the Atlantic (Docquier et al., 2022). Årthun et al. (2012) found based on observations that the Barents Sea lost 145,000 km^2 of SIA per 10 TW increase in OHT between 1998 and 2008, with OHT leading by 2 years and 70,000 km^2 of SIA per 10 TW increase in OHT between 1948 and 2008, with OHT leading by 1 year. These are annual mean values, but most of the sea ice loss in this region occurs in the winter ($> 50\%$ since 1979) (Onarheim and Årthun, 2017). Within the Atlantic Ocean, the Fram Strait and Davis Strait are the nest 2 biggest gateways of OHT to the Arctic, transport annual mean energy of 36TW and 20 TW of respectively (Docquier and Koenigk, 2021).

Dörr et al. (2024) find that influence of Atlantic and Pacific OHT will move polewards in the future, with increasing importance of inflows. Area impacted by Atlantic OHT becomes smaller, but that impacted by Pacific OHT becomes larger initially, but starts decreasing once total ice loss is achieved. But how the impact of OHT on Arctic sea ice variability will evolve in the future remains uncertain (Dörr et al., 2024).

1.4 Model uncertainty

Its has been shown by Mahlstein and Knutti (2011) that model simulations that have greater poleward OHT also depict larger future warming of the Arctic as well as globally. In these simulations, more solar radiation is absorbed by the now increased sea surface area, leading to further increase in global surface temperatures, and thus faster decline of sea ice. Mahlstein and Knutti (2011) thus propose that the complexity of this mechanism introduces uncertainties on modelling of future arctic sea ice, and will thus benefit from higher resolution and greater complexity of models.

A number of studies have investigates the ability of models to capture the complex relationships between Arctic sea ice and OHT, with most recent studies focusing on models that

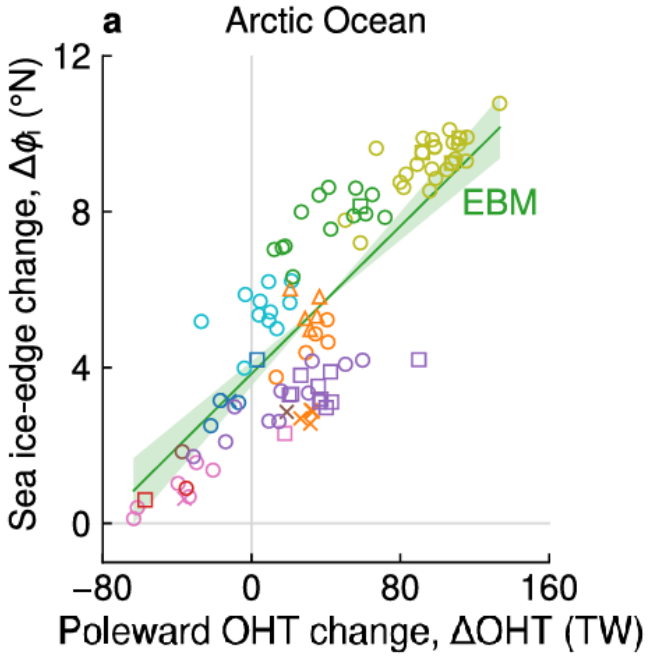

Figure 1.3: Change in Arctic ice edge latitude ($\Delta\phi$) plotted against change in poleward (ΔOHT, calculated at 65°N). Changes are the difference between 1980-2000 and 2030-2050 means. Each symbol refers to a different CMIP6 model. The green line and shaded region represent the linear relationship between the 2 quantities according to a theoretical EBM. *Source: Aylmer et al. (2024)*

are part of CMIP6 (Coupled Model Intercomparison Project-6). Lee et al. (2023) investigated 42 CMIP6 models and found that while multimodel means capture sea ice decline relatively well, its remains a challenge for individual models. Models with larger number of ensemble members have a larger chance of having at least one member that captures observed relationships between OHT and sea ice reasonably well.They also found that individual CMIP6 models that have a larger poleward OHT also simulate a larger Arctic sea ice decline, pointing to an emergent constraint in these models (also see Aylmer et al. (2022)).

Aylmer et al. (2022) analysed 20 CMIP6 models and found a similar strong relationship between poleward OHT and declining sea ice, for both hemispheres. But they found that the underlying mechanisms in both hemispheres were quiet different. In the Arctic, they found that increase in OHT in simulations results in increased convergence of ocean heat along the ice edge, nut has little effect on Arctic wide ice loss. Thinning of ice across central Arctic is primarily driven by increased poleward AHT convergence north or the ice edge.

Aylmer et al. (2024) analysed the change in ice-edge latitude, $\Delta\phi$ with changes in poleward

ocean heat transport, ΔOHT, from 20 models, and compared them to the energy balance model (EBM) derived by Aylmer et al. (2024) (Figure 1.3).

Thus, in this report we will analyse the relationships between OHT, AHT and ϕ in 4 individual CMIP6 models to try to further understand the underlying mechanisms in these models.

1.5 Scope and structure of report

As discussed in the previous sections in this chapter, a positive correlation between OHT and Arctic ice-edge latitude has already been established by a number of previous studies. The primary aim of this project is to investigate if a causal relationship between the 2 exists, and what the direction of causality might be, using lead/lag correlations. We will also look at the relative roles of AHT and OHT in driving sea ice changes, and the role of the AMOC as a possible mechanism for ocean heat transport towards the Arctic. We propose, similar to what Aylmer et al. (2024) say, that if changes in OHT lead those in sea ice, we would see it leading by a shorter time or 5-10 years. But if changes in sea ice lead, we should see it lead by a longer time ($\tilde{1}$5 years) since it would need to modify the entire thermohaline circulation, which drives the poleward OHT in the Atlantic. We will also choose to focus on the AMOC as a possible driver of OHT, because of constraints of this study, and because the Barents Sea, Fram Strait and Davis Strait, all part of the North Atlantic, are the biggest paths of OHT to the Arctic (see Section 1.3.1).

In this chapter we have already discussed the observed trends in past and present Arctic sea ice, the impacts of sea ice loss on the global climate and some possible feedback mechanisms such as ice-albedo feedback. We have also discussed various drivers of sea ice- global warming caused by anthropogenic CO_2 emissions, rise in near-surface air temperatures, Arctic cyclones and AHT. We then discussed the role of the ocean in transporting heat to the Arctic , future projections on sea ice decline and uncertainty in model projections.

In Chapter 2 we start off with a description of how relevant data was sourced for this study, the choice of models and description of various diagnostics used. We then explain how the AMOC index is calculated, followed by an explanation of the lead/lad correlations- calculation procedure, interpretation and choice of reference latitudes.

The results and discussion is presented in Chapter 3. We start by presenting time series

plots for our 4 models, for various relevant quantities and discussing the differences between trends across models. We then discuss the correlation maps of $\Delta\phi$ with ΔTAS, ΔOHT and ΔAHT. Then we present a short discussion on the possibility of the AMOC being a carrier of ocean heat to the Arctic. We conclude the chapter by presenting a possible mechanism of how the ocean drives changes in Arctic sea ice.

At the end, Chapter 4 contains our conclusions, a discussion on limitations of this study and ideas for future work.

Chapter 2

Data and Methodology

2.1 Data

For studying the dynamics of poleward heat transport and sea ice melting, we have used simulation data from 4 CMIP6 models- CanESM5, UKESM1-0-LL, MPI-ESM1-2-HR and CNRM-CM6-1. In addition, we have used observation data for OHT and ϕ in Section 2.1.2 to compare them to output from the models. CMIP6 diagnostics data for Ocean Heat Transport (OHT), Atmospheric Heat Transport (AHT), Ice Edge Latitude (ϕ) and near Surface Air Temperature (TAS) data was taken from Aylmer (2024). The same data archive also contains processed passive microwave observation data for ice-edge latitude. Observation data for ocean heat transport refers to the reanalysis data taken from Gael (2023). Table 2.1 contains a summary of variables obtained from each model, the source of data for this report and ensemble members used.

2.1.1 Climate Scenarios

We conduct our analysis using CMIP6 model data from the period 1850-2100. This comprises of 2 periods- *historical* (1850-2014) and *SSP3-7.0* (2015-2100).

The *historical* simulations are serve as a critical component in CMIP6 experiments by providing a baseline for evaluating climate models against observed data (Eyring et al., 2016). They can be used to asses how well climate models reproduce the observed climate of the recent past. The initialization starts from a specific point on from the *piControl* (pre-industrial control) simulations. The forcings- natural forcings such as volcanic eruptions and variations in solar energy, as well as anthropogenic forcings such as CO_2 emissions and land use, are

based on observations.

The *SSP3-7.0* scenario is a future climate scenario with medium to high end forcings (Eyring et al., 2016, O'Neill et al., 2016).

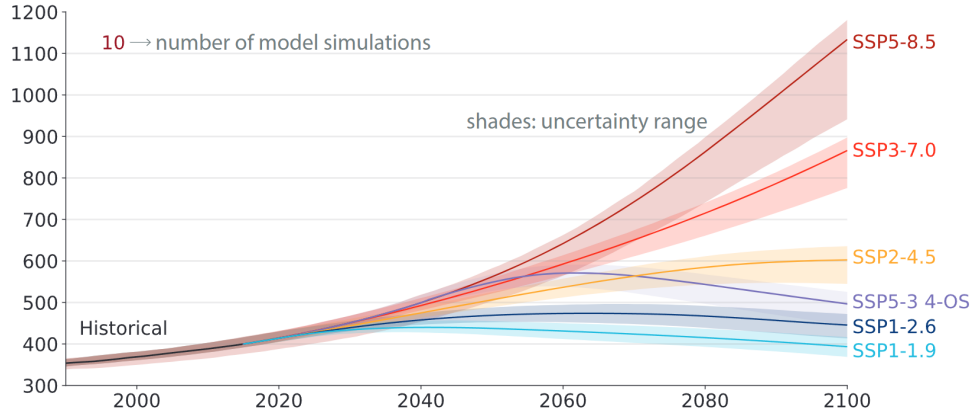

Figure 2.1: Future CO2 projections:projected CO2 concentrations (in ppm) in the Shared Socio-economic Pathway (SSP) scenarios in response to anthropogenic CO_2 emissions, from (**?**) and (**?**)

2.1.2 Choice of models

In this study, we have chosen 4 models from the CMIP6 archives for our analysis- CanESM5, UKESM1-0-LL, MPI-ESM1-2-HR and CNRM-CM6-1. Note that zonally integrated meridional overturning streamfunction (Ψ) data, which is used to calculate the AMOC index (2.2.4), is not available for CNRM-CM6-1 in CMIP6 archives. Every ensemble member of a model is denoted by a set of 4 IDs- initialization *i*, realization *r*, physics *p*, and forcing *f*. For each model, only those members are chosen for which values of all required quantities are available. Table 2.1 lists the chosen models and their ensemble members.

We have chosen these 4 models so as to cover a substantial range of model results from Figure 1.3. In this figure by Aylmer et al. (2024), showing chΔOHT and $\Delta\phi$ as the difference between means over 2030-2050 and 1980-2000, every point represents a member, and every symbol represents a distinct CMIP6 model. We have chosen the 4 models so as to cover a wide range of model types. CanESM5 (yellow circle) has the highest increase in OHT and highest sea ice loss and is also within range of the EBM. UKESM1-0-LL (green circle) has higher higher increase in OHT compared to the EBM and MPI-ESM1-2-HR (purple circle) has lower OHT increase. CNRM-CM6-1 (pink circle) is the only one of our chosen model to

have a decrease in OHT, but it closely follows the EBM.

Model	Variable	Source	Variable name in source	Ensemble members
CanESM5	OHT AHT TAS ϕ	Aylmer (2024)	*oht* *aht_n* *tas_n* *iel_zm_n*	r(1-25)i1p2f1
	Ψ	Swart et al. (2019)	*msftmz*	r(1-10)i1p2f1
UKESM1-0-LL	OHT AHT TAS ϕ	Aylmer (2024)	*oht* *aht_n* *tas_n* *iel_zm_n*	r(1-4,8-12,16-19)i1p1f2
	Ψ	Shim et al. (2020)	*msftyz*	
MPI-ESM1-2-HR	OHT AHT TAS ϕ	Aylmer (2024)	*oht* *aht_n* *tas_n* *iel_zm_n*	r(1-10)i1p1f4
	Ψ	Jungclaus et al. (2019)	*msftmz*	
CNRM-CM6-1	OHT AHT TAS ϕ	Aylmer (2024)	*oht_n* *aht_n* *tas_n* *iel_zm_n*	r(1-6)i1p1f4
Observations	OHT, ϕ	Aylmer (2024)		

Table 2.1: Summary of data used. Left to right: Model name as used in CMIP6 data archive, variable abbreviation/symbol as used in this report, source of data fro this study, variable name of data in source archive and Ensemble members (for CMIP6 data)

2.2 Diagnostics

2.2.1 Ice Edge Latitude, ϕ

These are annual mean values, computed from monthly-mean sea ice concentration fields, which are first linearly interpolated onto a regular, independent longitude/latitude grid of

similar resolution to the nominal ocean grid of each model. Then an algorithm is implemented that identifies the ice edge (15% concentration) latitude at each longitude, excluding such points that are too close to land as these obscure the seasonal cycle of ice cover in the final, zonal average metric. These calculations for the ice edge latitude for the 4 models used were done by Aylmer (2024) and all data has been sourced from their archive. For a mode detailed explanation of the algorithm, see Eisenman (2010).

The advantage of using sea ice-edge latitude over SIA or SIE is that removes the asymmetries in the seasonal cycle of Arctic sea ice cover that arise as a result of continental land distribution (Eisenman, 2010). At the multi-decadal timescales which are of interest in this study, the ice-edge latitude and SIA have a roughly 1:1 correspondence (correlation coefficient close to -1) (Aylmer et al., 2022). Thus, trends in ϕ, and its relationships to other dynamical properties of the atmosphere and ocean, that have been discussed in this report are representative of the trends and relationships of the total Arctic sea ice cover.

2.2.2 Ocean and atmospheric heat transports

For all 4 models, annual mean values of OHT and AHT are readily available in the archive (Aylmer, 2024).

For UKESM1-0-LL, CanESM5 and MPI-ESM1-2-HR, annual mean OHT data is available under 'hfbasin', which gives the net northward OHT integrated in depth, and within ocean basins (Aylmer et al., 2024). The horizontal integration is done along a zigzag path of native ocean grid cells, which lie approximately along latitude lines (Griffies et al., 2016). For CNRM-CM6-1, the OHT data is in 'hfx/hfy', which is an Arakawa-C grid with components of heat fluxes situated on the top and right edges of the grid cells (Voldoire et al., 2019, Aylmer et al., 2024).

For all models, (Aylmer et al., 2024) have calculated AHT (the total moist static energy transport) at a latitude as as integration of net heat flux into the atmosphere over all latitudes poleward of the reference latitude.

2.2.3 Average surface air temperature

The near-surface air temperature (TAS) is available at annual-mean frequency in the source archive (Aylmer, 2024). Its is the average temperature of near-surface air between the refer-

ence latitude and the North pole (in the northern hemisphere). See Aylmer et al. (2024) for more details on how it is calculated from CMIP6 model data.

2.2.4 AMOC index

The strength of the Atlantic Meridional Overturning Circulation (AMOC) can be measured using the AMOC index (Cheng et al., 2013, Latif et al., 2022), which is derived from the meridional overturning streamfunction, ψ. For a chosen reference latitude, the annual mean of ψ is first zonally integrated across the Atlantic ocean basin. The maximum in-depth value then gives us the AMOC index, at that reference latitude, in Svedrups (1 Sv= $10^6 m^3/s$).

If we assume that ψ=0 Sv at the bottom of the ocean (no slip condition) then at a given latitude, the AMOC index gives us the equator-ward volume below the depth at which the maximum value of ψ occurs. Thus, a positive AMOC index means that the net volume transport is towards equator and below this depth and poleward above it.

Since the AMOC index calculated in this way represents the total lower level volume transport at a given latitude, it can be used to represent the strength of the overall overturning circulation in the Atlantic. But there is still significant variation in the AMOC index values across latitudes. This variation and its effects are discussed further in Section 3.4.1.

2.3 Lead/Lag Correlations

2.3.1 Calculation

In Chapter 3, we present the relationships between various dynamical variables in the form of lead/lag correlations. Let us consider an example in which these 2 variables are A and B. Our aim is to see how changes in A and B (ΔA and ΔB respectively) are correlated to each other and how much time it takes for the signal from the changes in one quantity to affect the changes in the other. Each of these changes are calculated as the difference between the mean over 2 consecutive, non-overlapping, 20 year time periods. For every ensemble member of a model, we first fix ΔB to be the difference between means over 1981-2000 and 2001-2020 (i.e. centered at 2000),

$$\Delta B = \left\langle B \right\rangle_{2001}^{2020} - \left\langle B \right\rangle_{1980}^{2000} \tag{2.1}$$

Now we calculate a set of ΔA, each centered at 41 different years from 1980 to 2020.

$$\Delta A_t = \left\langle A \right\rangle_{(2001+t)}^{(2020+t)} - \left\langle A \right\rangle_{(1980+t)}^{(2000+t)}, \tag{2.2}$$

where t $\in$ [-20,20] is the time (in years) by which ΔB leads. For each ΔA_t, we calculate a Pearson correlation coefficient, r_t, with the fixed ΔB from Eq. 2.1, across ensemble members of a single model. We now get a series of correlation coefficients, r_t:

$$r_t = r[\Delta A_t, \Delta B] \tag{2.3}$$

Note that, in this report, whenever a lead/lag correlation is presented in the form like Eq. 2.3, ΔB is fixed in a time period. ΔA leads for t<0 and lags for t>0.

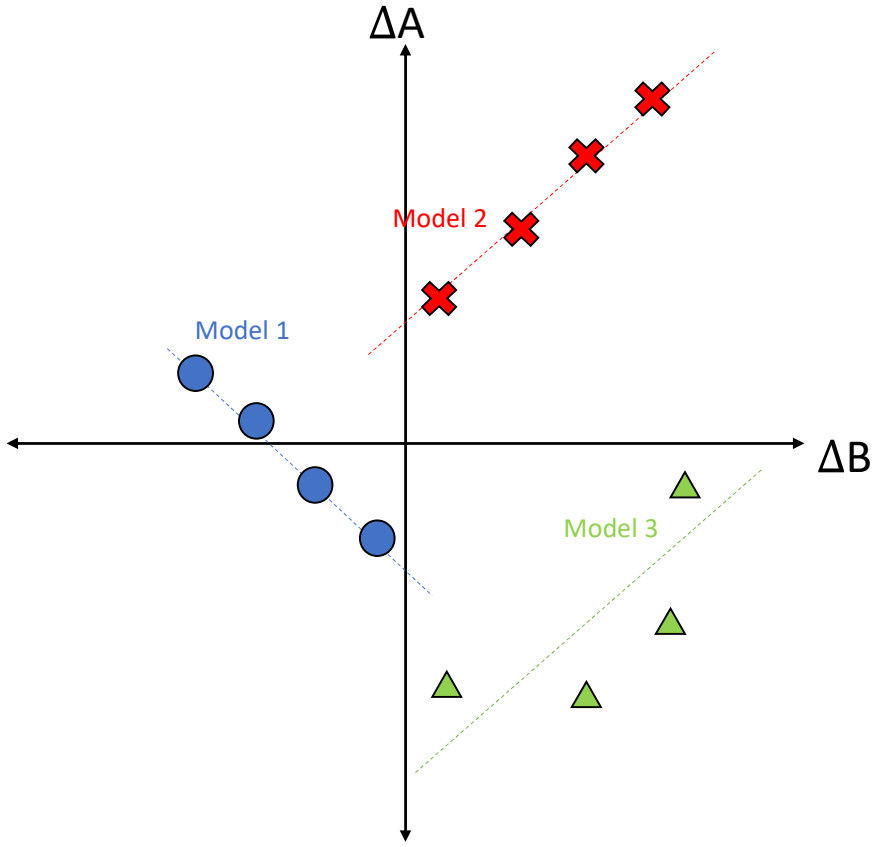

Figure 2.2: Example of how distribution of ensemble members within a model can affect the calculation of the Pearson correlation coefficient across ensemble members. Members of example Model 1, Model 2 and Model 3 are in blue circles, red crossed and green triangles respectively

2.3.2 Interpretation

To understand what a correlation across ensemble members of a model means, let us consider an example. In Figure 2.2, we plot ΔA vs ΔB values, at a chosen time, for ensemble members of 3 models, with correlation values r_1, r_2 and r_3. The Pearson correlation coefficient, r_i, ranges between -1 and 1. Its magnitude is a measure of how closely the distribution of members follows a linear relationship, and the sign gives the sign of the slope of this linear trend. In our example (Figure 2.2), assume that the r-values for each of the 3 models are $r_1 = -0.9$, $r_2 = 0.9$ and $r_3 = 0.35$ respectively. Model 1 and Model 2 both have the same magnitude of r, but their signs are opposite, indicating opposite slopes of linear trend. Model 3 has a much smaller value of r (=0.35), indicating that its members follow a weaker linear relationship. Note that $r_3 < r_2$, even though the slope of linear trends of Model 2 and Model 3 are the same. This is because the r-value does not provide any information about the magnitude of the slope of the linear trend.

A positive r means that within the model, increase in ΔA corresponds to increase in value of ΔB. A negative r means that increase in ΔA corresponds to a decrease in ΔB. But we cannot know whether A, B, ΔA or ΔB are increasing or decreasing unless we also look at the exact values of ΔA and ΔB from the time-series of A and B.

For example, all members of Model 2 show that an increase in A ($\Delta A > 0$) occurs with an increase in B($\Delta B > 0$). But according to Model 3, increase in A ($\Delta A > 0$) occurs with an decrease in B ($\Delta B < 0$). But both models have positive r-values. he sign of the r value does not give us any information about how A or B changes with time, or how A and B are correlated. Instead, it only gives us information on the relative behaviours of the changes in A and B.

Thus, in order to fully understand how A and B correlate to each other, we need to look at the time series of both quantities along with lead/lag correlations. In our discussion, we will look at the time series in Figure 3.1 for this. In the figure we only have the time series at a specific reference latitude (65°N for OHT, AHT and TAS; 26.5°N for AMOC index) and for the sake of simplicity, we will assume that the sign of ΔA and ΔB are the same for all reference latitudes. The implications of this assumption will be discussion in Chapter 4.

2.3.3 Choice of reference latitudes

For lead/lag correlation maps, the reference latitude range is chosen as 50°- 87°N for ΔOHT and ΔAHT and $50°N - 90°N$ for ΔTAS. The lower limit is $50°N$ because we are only interested in the total heat that is being transported to the Arctic sea ice. The surface air temperature or flow of heat across lower latitudes has no direct effect on the sea ice and correlation of those values with $\Delta\phi$ is of no use in this study. The upper limit chosen so because AHT and OHT data for latitudes north of $87°N$ is not available. When correlations are calculated for 2 quantities both of which require a reference latitude, we calculate with both quantities with reference latitudes varying together. For example, in Figure 3.5, the y-axis represents the reference latitude for both AHT and OHT.

Chapter 3

Results

Figure 3.1 presents the time series plots for various climate metrics across 4 CMIP6 models: CanESM5, UKESM1-0-LL, MPI-ESM1-2-HR, and CNRM-CM6-1, with observational data included for comparison. The metrics plotted are Ocean Heat Transport (OHT) in petawatts (PW), Atmospheric Heat Transport (AHT) in PW, surface air temperature (TAS) in Kelvin (K), the AMOC Index in Sverdrups (Sv), and the index ϕ in degrees north (°N). AHT, OHT and TAS are plotted at reference latitude 65°N and AMOC index at reference latitude 26.5°N.

The plot shows that CNRM-CM6-1 (red) is the only model with a notable decrease in OHT over time, in contrast to the other models which display a general increase. The black line representing observational data is closest to the MPI-ESM1-2-HR (green) model. The AHT plot displays relatively stable trends for all models, except for CNRM-CM6-1, where AHT sharply increase and decreases in the same period (2000-2100) as OHT does decreases and then increases for the same mode. UKESM1-0-LL, which has the strongest increase in OHT, also has the strongest decrease in AHT. This is indicative of the models being able to show the Bjerkness compensation, which will be discussed further in Section 3.3. The AMOC index shows a decline over time in the available models, with the MPI-ESM1-2-HR showing the most consistent long term trend. Compared to the other 3 models, MPI-ESM1-2-HR has smaller long term variations of other quantities as well, a possible reason for which could be its relatively finer spatial resolution.

The surface air temperature, TAS (mean surface air temperature between reference latitude and North pole), plots show a consistent increase across all models, with CanESM5 (yellow) showing the highest rise. The ϕ plot also has a sharp increase across the models, with UKESM1-0-LL (blue) and CanESM5 showing the highest changes. The observational

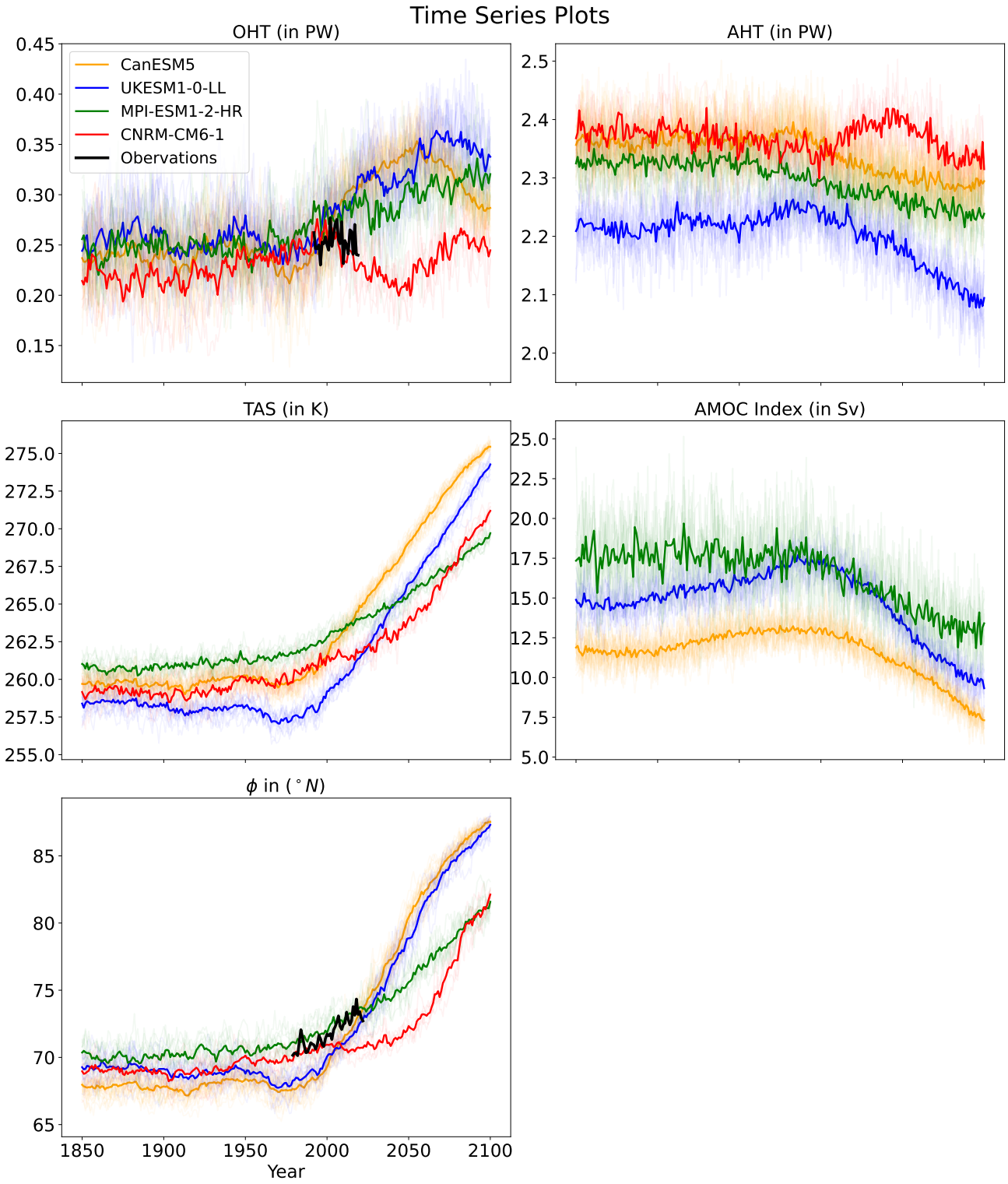

Figure 3.1: Time series of for 4 CMIP6 models. OHT, AHT and TAS are at 65°N. AMOC index at 26.5°N. Thick lines represent ensemble means and thin lines represent individual ensemble members. Member means and individual members are represented by same colour. Black line in OHT and ϕ plots represents observation data. AMOC index data not available for CNRM-CM6-1.

data (black line) fall within the variation range of the models, closely following the trend seen in MPI-ESM1-2-HR. The TAS and ϕ trends closely follow each other across all 4 models. This points to a strong link between the 2. As discussed in Sections 1.1 and 1.3, an increase in surface air temperature has been identified as the strongest driver if Arctic sea ice loss. Thus a strong relationship between ATS and ϕ in the models is consistent with previous findings. The relationship between TAS and ϕ will be discussed further in Section 3.1.

Overall, the figure underscores the variability across different climate models, with observational data generally falling within the ensemble spread. This variation is particularly pronounced in short-term inter-annual variability, which complicates the determination of which model best represents long-term trends.

3.1 Relationship between TAS and ϕ

The change in average surface air temperature has a strong positive correlation with the change in ice edge latitude (Figure 3.2). In all models, the correlation is strongest around 0 lead time, with $\Delta\phi$ leading at high latitudes in MPI-ESM1-2-HR and and ΔTAS leading slightly between $50°N$ and $60°N$ in UKESM1-0-LL. The correlation becomes weaker as the lead/lag period between the 2 quantities becomes greater. The near air surface temperature is an average over the the entire area between the reference latitude and the north pole, a huge part of which is covered by the sea ice itself. Therefore it is not surprising that changes in TAS and ϕ are coupled.

From Figure 3.1 we can see that the location of highest correlation in each model is close to the respective position of the mean ice edge latitude in during 1980-2020. From 3.1 we can also see that the plots between ϕ and TAS have the same trend in each model throughout the time domain. This strong correlation is also consistent with previous studies that have found increase of surface air temperature due to global warming to be the primary driver of Arctic sea ice loss (Johannessen et al., 2004, Notz and Marotzke, 2012, Docquier et al., 2022).

In CanESM5 and MPI-ESM1-2-HR, there is also a statistically significant negative correlation around $70°N$, with $\Delta\phi$ leading by 17-20 years. A possible reason for this could be that once the sea ice edge has retreated, the rate at which the surface temperature increases slows down. This is because the heat storage capacity of the now exposed ocean surface is much higher than the sea ice. Exposed sea surface can also dissolve more CO_2 from the atmosphere,

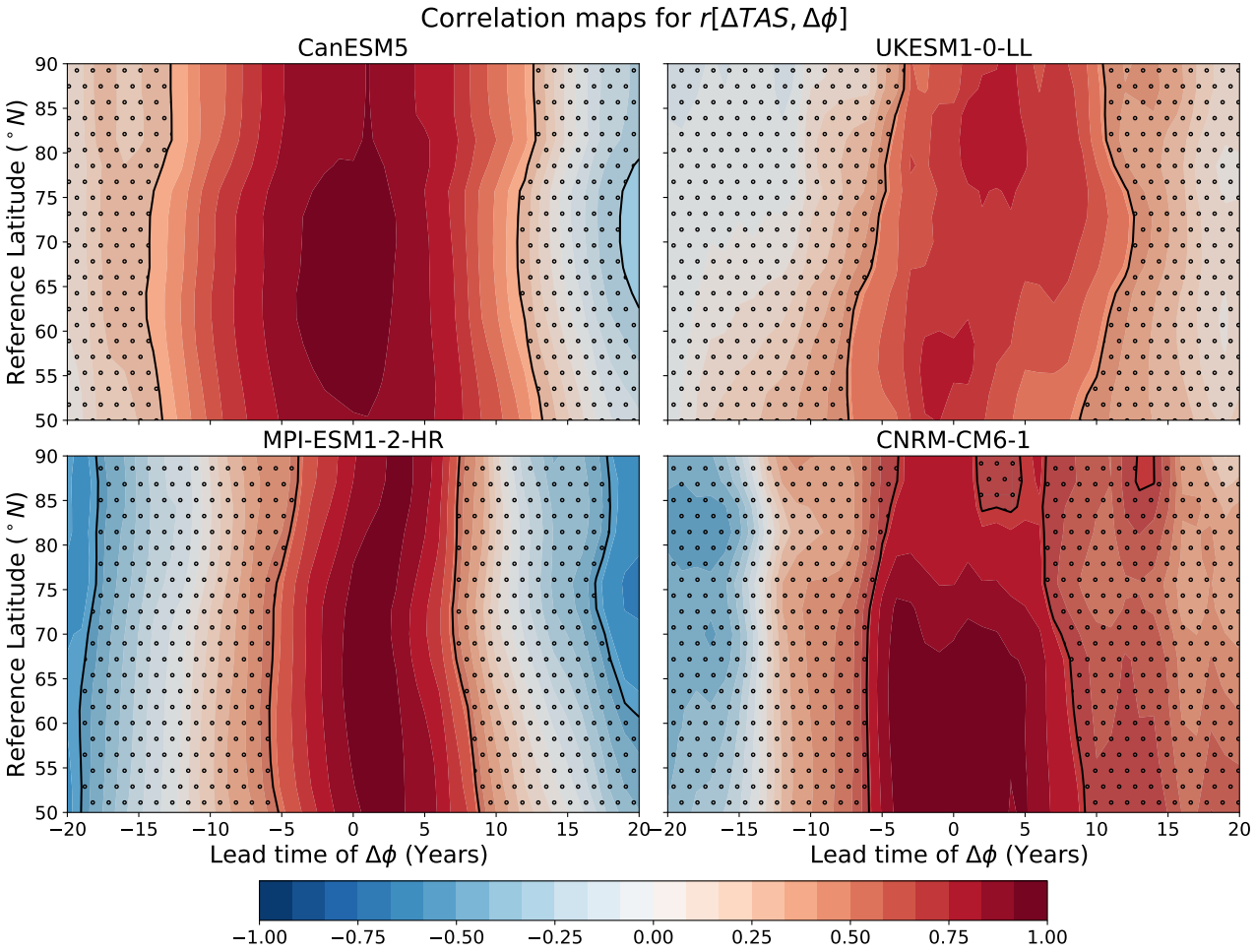

Figure 3.2: Correlation between ΔTAS and $\Delta\phi$. Colours represent the value of Pearson Correlation Coefficient, r[ΔTAS,$\Delta\phi$]. The stippled region has a p-value > 0.1 (level of significance$<$ 90%, calculated using a t-test). Vertical axis is the reference latitude at which TAS is calculated. Horizontal axis is the time (in years) by which $\Delta\phi$ leads ΔTAS.

further slowing down the rate of temperature rise (Ouyang et al., 2020).

3.2 Correlation between of OHT and ϕ

We will now look at the relationship between changes in poleward OHT and ice-edge latitude. Figure 3.3 shows the lead-lag correlation maps for the 4 CMIP6 models. Note that the correlations in the stippled regions (p$>$0.1) should be interpreted with caution, but not entirely ignored. As discussed in Section 2.3, we interpret these correlations along side the time series in Figure 3.1. From this figure we can see that both OHT and ϕ are increasing in time for all models, that is, ΔOHT > 0 and $\Delta\phi > 0$. Therefore, a positive correlation between ΔOHT

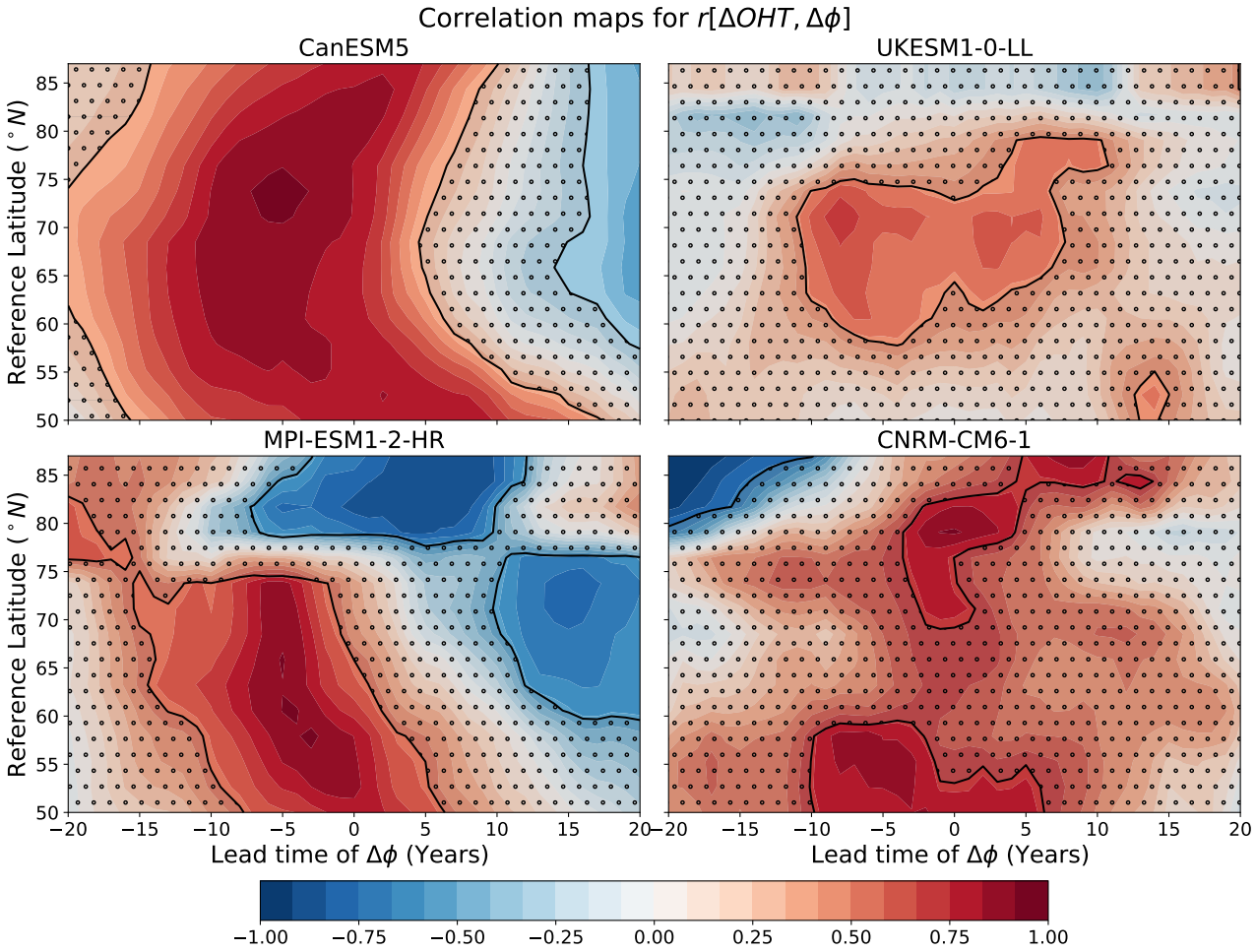

Figure 3.3: Correlation between ΔOHT and $\Delta\phi$. Colours represent the value of Pearson Correlation Coefficient, r[ΔOHT,$\Delta\phi$]. The stippled region has a p-value > 0.1 (level of significance$<$ 90%, calculated using a t-test). Vertical axis is the reference latitude at which OHT is calculated. Horizontal axis is the time (in years) by which $\Delta\phi$ leads ΔOHT.

and $\Delta\phi$ means that, for a model, a stronger increase in OHT corresponds to a stronger increase in ϕ. Similarly, a negative correlation means that a stronger ΔOHT corresponds to a weaker $\Delta\phi$ in the model.

The region of maximum positive correlation is between 70°N and 80°N latitudes in CanESM5, between 65°N and 75°N in UKESM1-0-LL, between 55°N and 70°N in MPI-ESM1-2-HR and between 55°N and 60°N and 75°N and 80°N in CNRM-CM6-1. In all models, ΔOHT leads $\Delta\phi$ by 3-10 years. This is consistent with findings of Aylmer et al. (2024), who found that $\Delta\phi$ leads ΔOHT by around 5 years. But they have calculated these correlations across ensemble members of 20 CMIP6 models, whereas here we are able to show

that a similar relationship exists within some of the individual models as well.

From the same figure we can also see that, in CanESM5 and MPI-ESM1-2-HR, there is a statistically significant negative correlation, with $\Delta\phi$ leading ΔOHT by 15-20 years. This indicates that at longer time periods, changes in ϕ start leading changes in OHT, and that an increase in rate of sea ice changes in these models leads to slower change in OHT.

In MPI-ESM1-2-HR, the correlation become strongly negative north of about 77°N latitude, with $\Delta\phi$ leading by 5-10 years. This inversion of the correlation is also present in UKESM1-0-LL, but is statistically insignificant. This means that in these models, at higher latitudes, an increase in strength of change in ϕ leads to decrease in rate of OHT change. From Figure 3.1 we can see that OHT and ϕ are increasing in the chosen time period, we can say that a faster decline in sea ice is leading to a slower increase in OHT above 77°N in these 2 models.

We can see from Figure 3.1 OHT in the Atlantic ocean (across $65°N$) starts decreasing in the future. This happens around 2050 in CanESM5, 2060 in UKESM1-0-LL and about 2080 in CNRM-CM6-1. But the ice edge latitude keeps retreating, though at a slower rate. A similar phenomenon can also be seen between the years 2000 and 2050 in CNRM-CM6-1, where OHT decreases sharply and rate of ice-edge retreat decrease along with it. This shows us that the changes in sea ice are not dependent on changes on OHT alone. In following sections, we will see that $\Delta\phi$ has also has strong relationships with poleward ΔAHT, ΔTAS and ΔAMOC index. But for most of the *historical* period, changes in ϕ closely follow changes in poleward OHT in all models. Thus a change in this relationship in the future projection implies that with climate change, the dependence of ϕ on OHT may become less important. This is consistent with findings of Bitz et al. (2005) who concluded that under increasing CO_2 forcings, the convergence of OHT near the ice edge decreases.

3.3 Relationship between AHT and ϕ

We will now look at the relationship of AHT with ϕ and OHT. This, along with the results in the above section will help us understand the relative roles of the atmosphere and ocean in bringing heat to the Arctic and driving sea ice changes. From Figure 3.1 we can see that AHT is always decreasing (ΔAHT < 0). Thus r > 0 means that a stronger change (decrease) in OHT corresponds to a weaker change (increase) in OHT and ϕ, and r < 0 means that a

stronger change (decrease) in AHT corresponds to a stronger change (increase) in OHT and ϕ.

Exceptions to this are UKESM1-0-LL between 1950-1980 and in CNRM-CM6-1 between 2000 and 2050, where ΔAHT > 0. This will invert the interpretation of r[ΔAHT,$\Delta\phi$] when ΔAHT is leading in UKESM1-0-LL, and in when $\Delta\phi$ is leading in CNRM-CM6-1. Interestingly, both these region have mostly statistically insignificant correlation according to Figure 3.4. This could be because of large intra-model spread of members around the time when AHT trend shifts in these 2 models. But this not affect r[ΔOHT,ΔAHT] because in this case ΔAHT is fixed as the difference between means over 1981-2000 and 2001-2020 and is thus negative.

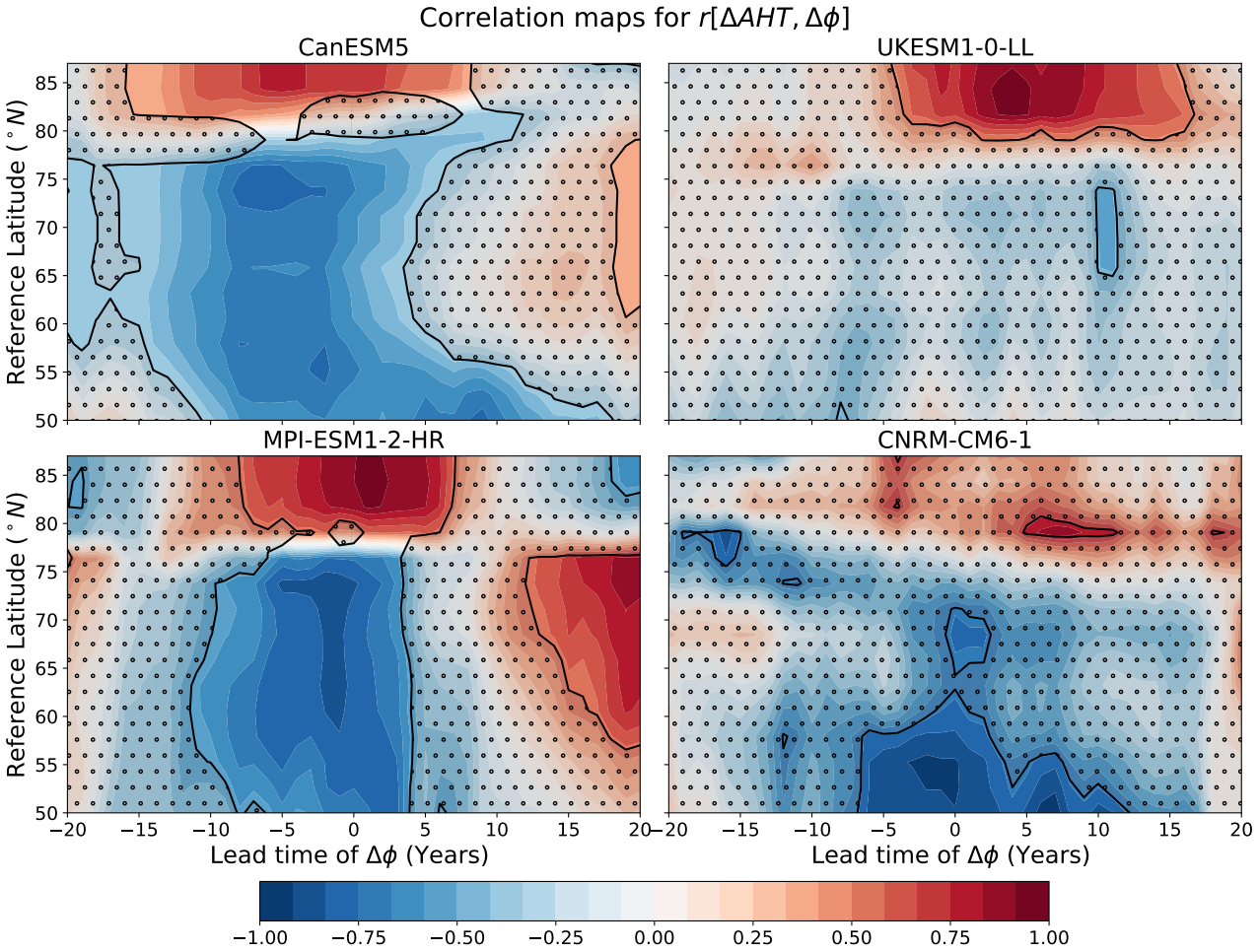

Figure 3.4: Correlation between ΔAHT and $\Delta\phi$. Colours represent the value of Pearson Correlation Coefficient, r[ΔAHT,$\Delta\phi$]. The stippled region has a p-value > 0.1 (level of significance$<$ 90%, calculated using a t-test). Vertical axis is the reference latitude at which AHT is calculated. Horizontal axis is the time (in years) by which $\Delta\phi$ leads ΔAHT.

South of about 80°N, there is a strong negative correlation between change in poleward AHT and change in ice edge latitude (Figure 3.4), with strongest correlation between 70°N and 75°N in CanESM5, 60°N and 75°N in MPI-ESM1-2-HR and 55°N and 60°N in CNRM-CM6-1. At these latitudes, ΔAHT leads $\Delta\phi$ by 0-6 years, showing that changes in AHT are leading changes in sea ice. Therefore, as the rate of decrease of AHT becomes stronger (south of 80°N), the rate of ice edge retreat also become stronger.

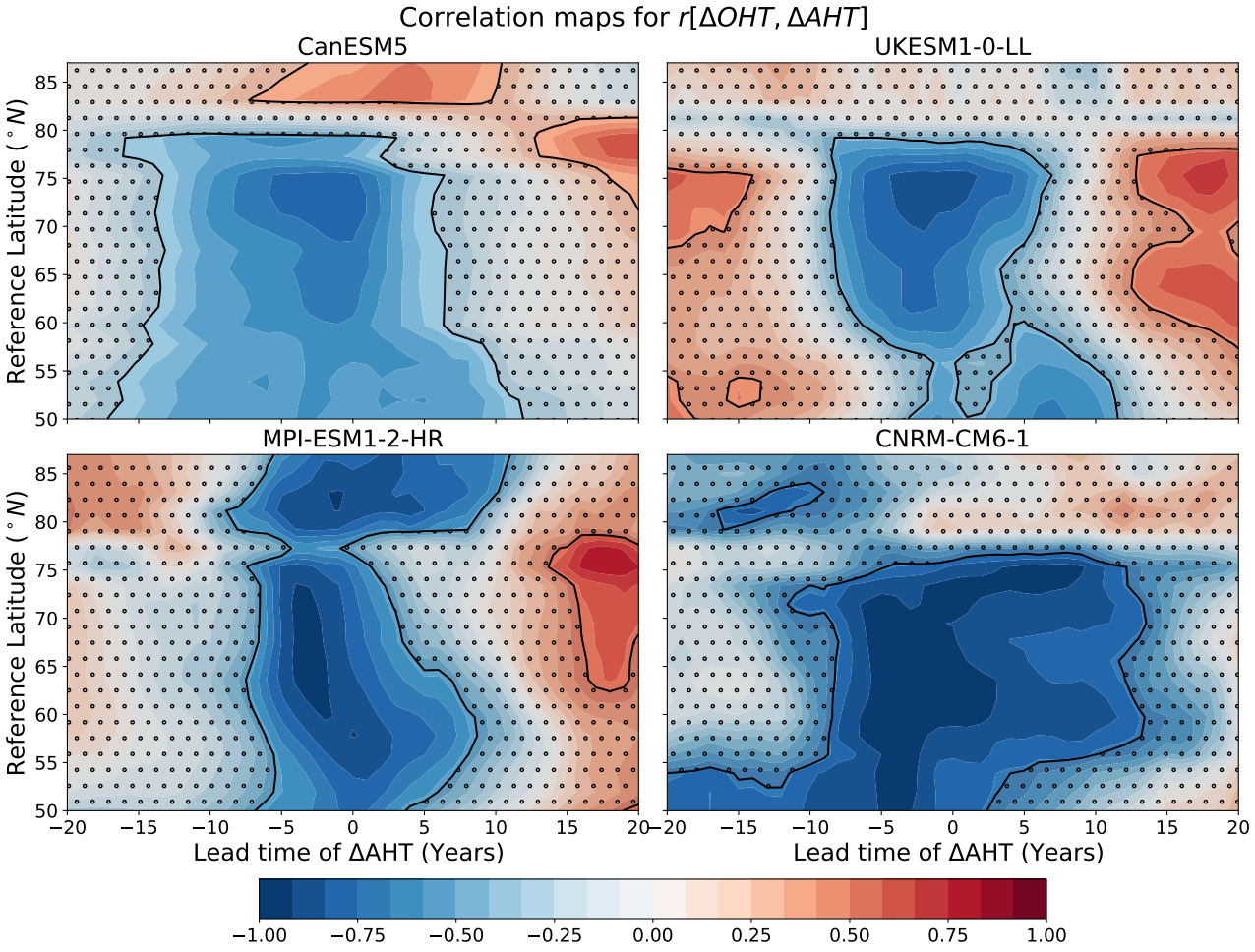

Figure 3.5: Correlation between ΔOHT and ΔAHT. Colours represent the value of Pearson Correlation Coefficient, r[ΔOHT,ΔAHT]. The stippled region has a p-value $>$ 0.1 (level of significance$<$ 90%, calculated using a t-test). Vertical axis is the reference latitude at which OHT and AHT are calculated. Horizontal axis is the time (in years) by which ΔAHT leads ΔOHT.

North of 80°N, the correlation becomes strongly positive, which means that an increase in AHT leads to decrease in sea ice. The reference latitudes at which this shift occurs varies across models. In each model, this latitude also changes with time, and trend of this shift is

similar to that of ϕ in Figure 3.1. It moves northwards in time fr CanESM5 and UKESM1-0-LL and moves slightly southward in CNRM-CM6-1. The latitude of shift remains mostly constant in MPI-ESM1-2-HR, similar to its ϕ, which has the weakest slope in time. This indicates that the shift sign of correlation is related to where the ice edge starts.

Correlation between ΔAHT and ΔOHT is strongly negative at latitudes south of 80°N in all 4 models. Since OHT is increasing in time and AHT is decreasing in time (Figure 3.1), this means that a stronger increase in OHT corresponds to a stronger decrease in AHT. The peak of negative correlations suggest thatΔOHT leads by 0-5 years in all models, except in CNRM-CM6-1, where ΔAHT starts leading north of 70°N. This negative correlation is the consequence of the models being able to simulate the Bjerknes compensation (Bjerknes, 1964). What Bjerknes compensation means is that if the top-of-atmosphere heat fluxes, and total heat content of the Earth's climate system remain constant, the total meridional heat transport should remain constant. This phenomenon appears as the negative correlation between ΔAHT and ΔOHT in our models.

Following this energy balance, and the correlation maps of r[ΔOHT,$\Delta\phi$] and r[ΔAHT,$\Delta\phi$], the correlation between ΔOHT and ΔAHT flips sign north of 75-80°N. Note that this flip does not occur in MPI-ESM1-2-HR because it is the only model which has significant negative correlation between ΔOHT and $\Delta\phi$ at high latitudes.

These correlations suggest a similar mechanism to the one proposed by Aylmer et al. (2022) for the northern hemisphere sea ice melting. South of where the ice edge occurs, changes in OHT are the primary driver of sea ice decline. Within this region, a negative correlation between changes in AHT and ϕ exists due to Bjerknes compensation. Near the ice-edge, the correlations become very weak. Here part of the OHT is converted to poleward AHT in the form of moist static energy. North or the ice edge, the heat is distributed across central Arctic via AHT, and thus we see a strong positive correlation between ΔAHT and $\Delta\phi$.

3.4 AMOC

3.4.1 Variation of AMOC with latitude

The AMOC index (Section 2.2.4) represents the meridional overturning volume transport across the reference latitude. The total volume of water transported meridionally does not stay

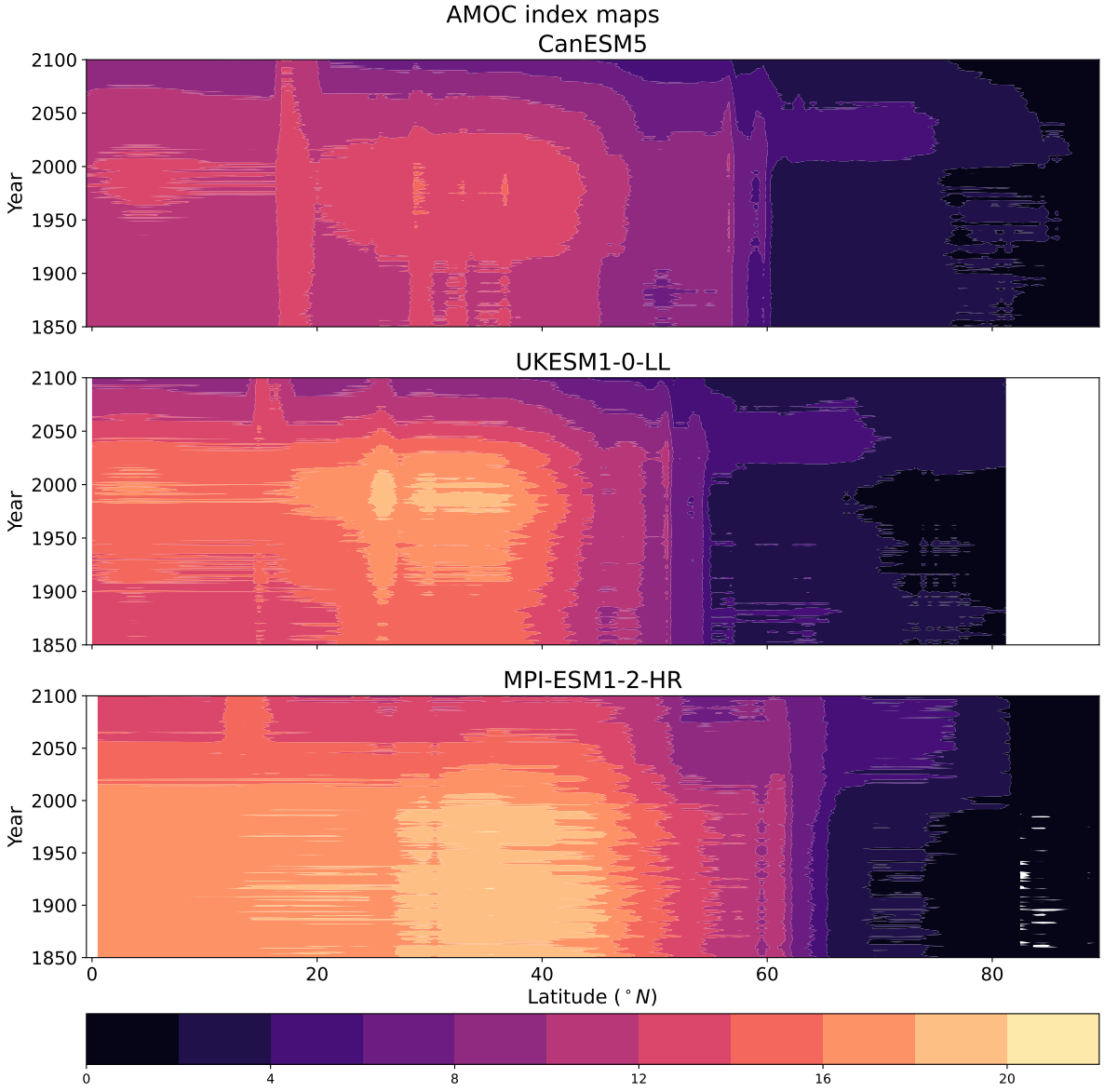

Figure 3.6: Variation of the AMOC index with time and latitude.

the same across latitudes since water is constantly being added to the ocean via precipitation, continental inflow from rivers, land ice melting etc., and being lost to evaporation. Thus, the choice of reference latitude can have a considerable effect on the AMOC index and is thus important for us to choose a reference latitude at which the index most accurately represents the strength of the overall overturning circulation.

Figure 3.6 shows how the AMOC index changes with reference latitude and with time. In all 3 models, its value is positive everywhere. This means zonal mean lower level flow is towards the equator at all latitudes in the Atlantic. Across latitudes, the values peaks at around 28°N in CanESM5, around 26°N in UKESM1-0-LL and around 35°N in MPI-ESM1-

2-HR. There is a strong drop in the AMOC index value at around 60°N in CanESM5 and MPI-ESM1-2-HR, and at around 55°N in UKESM1-0-LL. This sudden drop in the AMOC index occurs at 10°-15° south of where the ice edge occurs. South of this drop, the AMOC index increases in time in CanESM5 and UKESM1-0-LL, peaks at around 2000 and then goes back down to a minimum at 2100. In MPI-ESM1-2-HR, the change in AMOC index in time is slower. We can also see in Figure 3.1 that the slope of the AMOC time series for MPI-ESM1-2-HR is the weakest.

3.4.2 Relationship with poleward OHT

When we calculate r[ΔAMOC,ΔOHT], ΔOHT is fixed at the 1981-2000 and 2001-2020 period. Therefore ΔOHT is always positive. For MPI-ESM1-0-LL, ΔAMOC is always negative (Figure 3.1). For the other 2 models, ΔAMOC is positive only when it is leading by 15-20 years, close to 0 Sv at around 0 years lead time and negative after that.

In CanESM5 and and UKESM1-0-LL, there is a strong positive correlation north of 65°N, but from Figure 3.6 we know that the AMOC index has very low values at these latitudes. ΔAMOC is leading in CanESM5 and ΔOHT is leading in UKESM1-0-LL, which makes it uncertain which if these 2 is leading. The strong positive correlations mean that a stronger increase in OHT corresponds to a weaker decrease in the AMOC index. In UKESM1-0-LL, there is a strong negative correlation with ΔOHT leading. This means that a stronger increase in OHT leads to a stronger decrease in the AMOC strength after 15-20 years.

The sign of the correlations in MPI-ESM1-0-LL is opposite to those in the other 2 models. There is a strong negative correlation, a peak between 50°N and 55°N. ΔAMOC is leading ΔOHT be 0-15 years. This means that a stronger weakening of the AMOC leads to a stronger increase in OHT after 0-15 years. This result is completely opposite to the other 2 models.

Because of such strong disagreements between models, it is not possible to ascertain a definite correlation between OHT and the AMOC index, except fro what we can see from their time series in Figures 3.1 and 3.6- that poleward OHT becoming stronger under climate change co-occurs with AMOC becoming weaker in the long term.

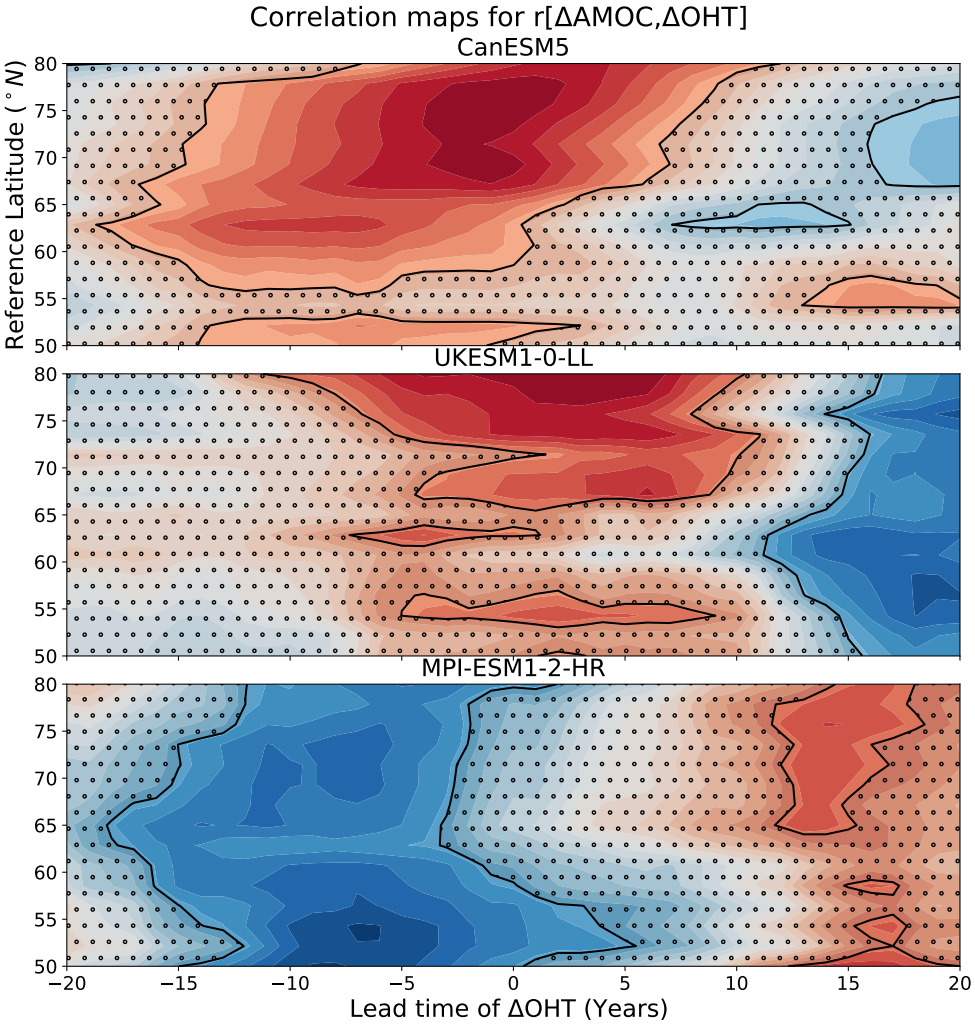

Figure 3.7: Correlation between ΔAMOC and ΔOHT. Colours represent the value of Pearson Correlation Coefficient, r[ΔAMOC,ΔOHT]. The stippled region has a p-value > 0.1 (level of significance$<$ 90%, calculated using a t-test). Vertical axis is the reference latitude at which OHT and AMOC index are calculated. Horizontal axis is the time (in years) by which ΔOHT leads ΔAMOC.

3.4.3 Relationship between AMOC and ϕ

There is a positive correlation between ΔAMOC and $\Delta\phi$ in CanESM5 and MPI-ESM1-2-HR, with strongest values between 65°N and 78°N and ΔAMOC leading by 0-7 years. The correlations in UKESM-1-0-LL are too weak and statistically insignificant. These correlations tell us that a stronger weakening of the AMOC leads to a weaker retreat in sea ice latitude, ϕ.

Therefore, we can say that AMOC is strongly correlated to Arctic sea ice retreat, and even tho OHT is also strongly correlated to ϕ, we cannot establish a causal pipeline mechanism

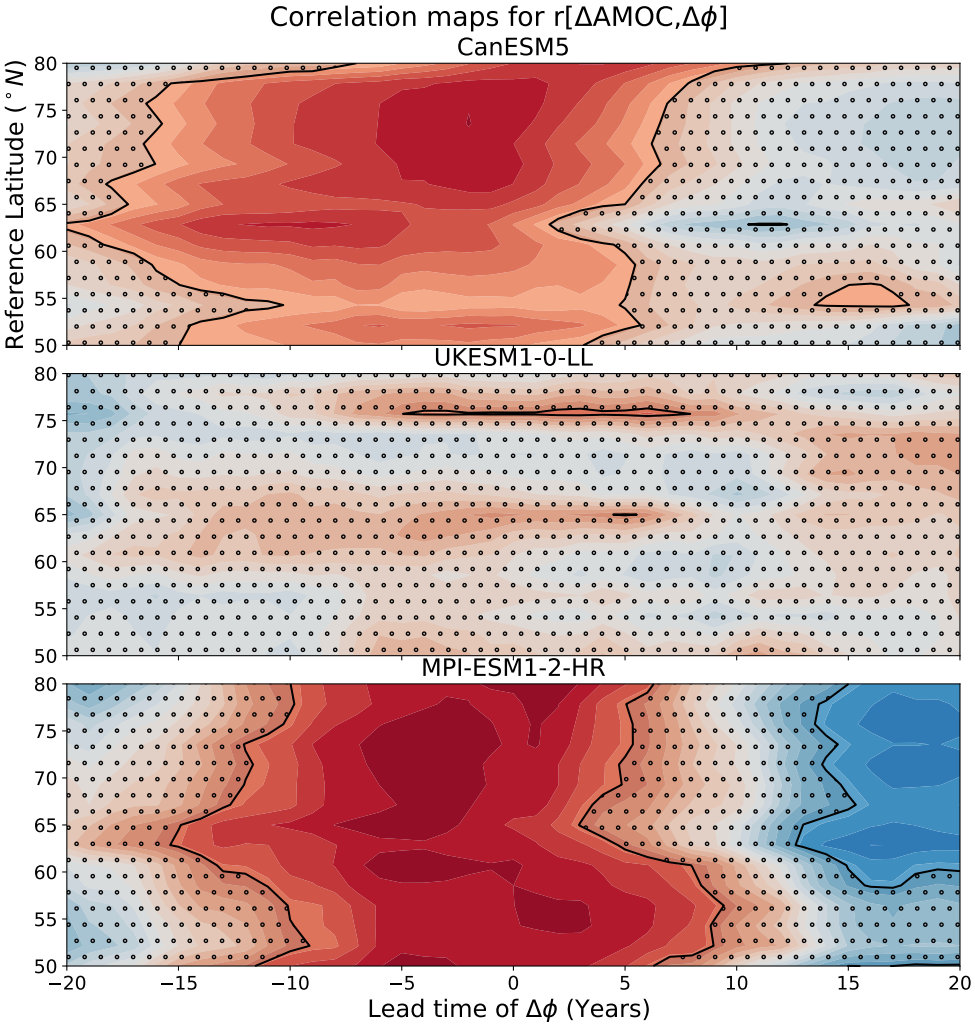

Figure 3.8: Correlation between ΔAMOC and $\Delta\phi$. Colours represent the value of Pearson Correlation Coefficient, r[ΔAMOC,$\Delta\phi$]. The stippled region has a p-value $>$ 0.1 (level of significance$<$ 90%, calculated using a t-test). Vertical axis is the reference latitude at which AMOC index is calculated. Horizontal axis is the time (in years) by which $\Delta\phi$ leads ΔAMOC.

linking these 3 since the correlation between AMOC index and OHT has a very wide inter-model spread.

Chapter 4

Conclusions and Future Work

4.1 Conclusions

We have analysed the relationships between meridional ocean heat transport, meridional atmospheric heat transport and average surface air temperatures with Arctic sea ice-edge latitude using 4 CMIP6 models- CanESM5, UKESM1-0-LL, MPI-ESM1-2-HR and CNRM-CM6-1. Our key findings are-

- A strong positive correlation exists between TAS and ϕ across all latitudes, with almost no lead or lag time. This is consistent with almost all previous studies that have established a strong link between rising global surface temperatures and Arctic sea ice loss.

- ΔOHT is has a strong positive correlation with $\Delta\phi$ south of ice edge location and strongly negative north of it. OHT changes lead by 2-7 years, which supports our hypothesis that OHT is driving sea ice changes. But in some models we can also sea a strong negative correlation with $\Delta\phi$ leading by 15-20 years, which would indicate that sea ice loss is driving observed changes in OHT. But the later result is not consistent across models.

- ΔAHT has the opposite trend of correlations with $\Delta\phi$, which is consistent with Bjerknes compensation. These correlations support the mechanism for Arctic ice melting as proposed by Aylmer et al. (2022), which says that OHT remains the primary carrier of heat to the Arctic south of the ice edge location. At the edge, the heat it transported to the atmosphere which then distributes it over central Arctic.

- The AMOC has a strong correlation with ϕ but its relationship with OHT has large inter-model spread. Thus we can see that changes in the AMOC does have a correlation with changes in Arctic sea ice, but the underlying mechanism of this relationship remains unknown in this study.

4.2 Limitations and Future work

All our analysis in this report has been done on model simulations, and out conclusions may not very well apply to real the real world. We have also chosen a specific future scenario- SSP3.7-0, but the relationship between OHT and ϕ may be different under different scenarios. Thus a more detailed analysis would require analysing more future scenarios.

We have limited out study to 4 CMIP6 models (3 for AMOC analysis), which severely limits our scope. In future work, it would be beneficial to look at a larger number of models.

We are only using zonal mean values of OHT, AHT, TAS, AMOC index and ϕ, which hides smaller scale processes and zonal variation. Future work should try to ficus on individual ocean basins in the Atlantic as well as Pacific.

For the interpretation of the lead/lag correlations, we have assumed the signs of changes of all quantities to be the same across all latitudes to what we can see at one latitude in 3.1. This is a very crude assumption and it would help to know the sign if change of both quantities at every point in a lead/lag correlation map for better interpretation.

Lack of number of models analysed has kept the role of AMOC in driving Arctic sea ice changes uncertain, and looking at results from more model should hep with better understanding if underlying mechanisms. Since the AMOC does not seem to be driving changes in the OHT, it is worth looking at other mechanisms that could be driving the changes. For example- wind driven gyres in the Atlantic and Pacific oceans.

Though lead/lag correlations can indicate what the direction of causality between changes in OHT and ϕ might be, they cannot prove it. We need to analyse underlying mechanisms of OHT across a large number of models and large number of initialisation and forcing variations to prove caustion for sure.

References

Aylmer, J., 2024: Diagnostics from cmip6, atmospheric reanalyses, and passive-microwave observations used to examine the impact of ocean heat transport on arctic and antarctic sea ice. University of Reading, URL https://doi.org/10.17864/1947.001333, doi:10.17864/1947.001333.

Aylmer, J., D. Ferreira, and D. Feltham, 2022: Different mechanisms of arctic and antarctic sea ice response to ocean heat transport. *Climate Dynamics*, **59**, 315–329, doi:10.1007/s00382-021-06131-x.

Aylmer, J. R., D. Ferreira, and D. L. Feltham, 2024: Impact of ocean heat transport on sea ice captured by a simple energy balance model. *Communications Earth Environment*, **5**, 406, doi:10.1038/s43247-024-01565-7, URL https://www.nature.com/articles/s43247-024-01565-7.

Bitz, C. M., M. M. Holland, E. C. Hunke, and R. E. Moritz, 2005: Maintenance of the sea-ice edge.

Bjerknes, J., 1964: Atlantic air-sea interaction. *Advances in Geophysics*, **10**, 1–82, doi:10.1016/S0065-2687(08)60005-9.

Cai, Q., J. Wang, D. Beletsky, J. Overland, M. Ikeda, and L. Wan, 2021: Accelerated decline of summer arctic sea ice during 1850-2017 and the amplified arctic warming during the recent decades. IOP Publishing Ltd, doi:10.1088/1748-9326/abdb5f.

Cheng, W., J. C. Chiang, and D. Zhang, 2013: Atlantic meridional overturning circulation (amoc) in cmip5 models: Rcp and historical simulations. *Journal of Climate*, **26**, 7187–7197, doi:10.1175/JCLI-D-12-00496.1.

Clancy, R., C. M. Bitz, E. Blanchard-Wrigglesworth, M. C. Mcgraw, and S. M. Cavallo, 2022: A cyclone-centered perspective on the drivers of asymmetric patterns in the atmosphere and sea ice during arctic cyclones. *JOURNAL OF CLIMATE*, **35**, 73–89, doi:10.1175/JCLI-D-21-0093.1, URL https://doi.org/10.1175/JCLI-D-21-0093.1.

Comiso, J. C., C. L. Parkinson, R. Gersten, and L. Stock, 2008: Accelerated decline in the arctic sea ice cover. *Geophysical Research Letters*, **35**, doi:10.1029/2007GL031972.

Docquier, D., and T. Koenigk, 2021: A review of interactions between ocean heat transport and arctic sea ice. IOP Publishing Ltd, doi:10.1088/1748-9326/ac30be.

Docquier, D., S. Vannitsem, F. Ragone, K. Wyser, and X. S. Liang, 2022: Causal links between arctic sea ice and its potential drivers based on the rate of information transfer. *Geophysical Research Letters*, **49**, doi:10.1029/2021GL095892.

Dörr, J., M. Årthun, T. Eldevik, and A. B. Sandø, 2024: Expanding influence of atlantic and pacific ocean heat transport on winter sea-ice variability in a warming arctic. *Journal of Geophysical Research: Oceans*, **129**, doi:10.1029/2023JC019900, on the Atlantic side, the impact of OHT moves northwards as the ice edge moves northwards in all models.

Eisenman, I., 2010: Geographic muting of changes in the arctic sea ice cover. *Geophysical Research Letters*, **37**, doi:10.1029/2010GL043741.

Eyring, V., S. Bony, G. A. Meehl, C. A. Senior, B. Stevens, R. J. Stouffer, and K. E. Taylor, 2016: Overview of the coupled model intercomparison project phase 6 (cmip6) experimental design and organization. *Geoscientific Model Development*, **9**, 1937–1958, doi:10.5194/gmd-9-1937-2016.

Fetterer, F., K. Knowles, W. N. Meier, M. Savoie, and A. K. Windnagel, 2017: Sea ice index, version 3. National Snow and Ice Data Center.

Francis, J. A., and B. Wu, 2020: Why has no new record-minimum arctic sea-ice extent occurred since september 2012? IOP Publishing Ltd, doi:10.1088/1748-9326/abc047.

Gael, 2023: Ecco v4 standard analysis sample (v4r5-rc2). Zenodo, URL https://doi.org/10.5281/zenodo.7869067, doi:10.5281/zenodo.7869067.

Griffies, S. M., and Coauthors, 2016: Omip contribution to cmip6: Experimental and diagnostic protocol for the physical component of the ocean model intercomparison project. *Geoscientific Model Development*, **9**, 3231–3296, doi:10.5194/GMD-9-3231-2016.

Hay, S., and Coauthors, 2022: Separating the influences of low-latitude warming and sea ice loss on northern hemisphere climate change. *Journal of Climate*, **35**, 2327–2349, doi:10.1175/JCLI-D-21-0180.1.

Johannessen, O. M., and Coauthors, 2004: Arctic climate change: observed and modelled temperature and sea-ice variability. *Tellus A: Dynamic Meteorology and Oceanography*, **56**, 328, doi:10.3402/tellusa.v56i4.14418.

Jungclaus, J., and Coauthors, 2019: Mpi-m mpiesm1.2-hr model output prepared for cmip6 cmip. Earth System Grid Federation, URL https://doi.org/10.22033/ESGF/CMIP6.741, doi:10.22033/ESGF/CMIP6.741.

Karami, M. P., T. Koenigk, and B. Tremblay, 2023: Variability modes of september arctic sea ice: drivers and their contributions to sea ice trend and extremes. *Environmental Research: Climate*, **2**, 025 005, doi:10.1088/2752-5295/accbe3.

Latif, M., J. Sun, M. Visbeck, and M. H. Bordbar, 2022: Natural variability has dominated atlantic meridional overturning circulation since 1900. *Nature Climate Change*, **12**, 455–460, doi:10.1038/s41558-022-01342-4.

Lee, Y. J., M. Watts, W. Maslowski, J. C. Kinney, and R. Osinski, 2023: Assessment of the pan-arctic accelerated rate of sea ice decline in cmip6 historical simulations. 6069–6087, doi:10.1175/JCLI-D-21, URL https://doi.org/10.1175/JCLI-D-21-.

Li, S., and W. Liu, 2022: Impacts of arctic sea ice loss on global ocean circulations and interbasin ocean heat exchanges. *Climate Dynamics*, **59**, 2701–2716, doi:10.1007/s00382-022-06241-0.

Liu, J., M. Song, Z. Zhu, R. M. Horton, Y. Hu, and S. P. Xie, 2022: Arctic sea-ice loss is projected to lead to more frequent strong el niño events. *Nature Communications*, **13**, doi:10.1038/s41467-022-32705-2.

Liu, Z., and Coauthors, 2021: Acceleration of western arctic sea ice loss linked to the pacific north american pattern. *Nature Communications*, **12**, doi:10.1038/s41467-021-21830-z.

Mahlstein, I., and R. Knutti, 2011: Ocean heat transport as a cause for model uncertainty in projected arctic warming. *Journal of Climate*, **24**, 1451–1460, doi:10.1175/2010JCLI3713.1.

Notz, D., and J. Marotzke, 2012: Observations reveal external driver for arctic sea-ice retreat. *Geophysical Research Letters*, **39**, doi:10.1029/2012GL051094.

Onarheim, I. H., and M. Årthun, 2017: Toward an ice-free barents sea. *Geophysical Research Letters*, **44**, 8387–8395, doi:10.1002/2017GL074304, URL https://onlinelibrary.wiley.com/doi/full/10.1002/2017GL074304https://onlinelibrary.wiley.com/doi/abs/10.1002/2017GL074304https://agupubs.onlinelibrary.wiley.com/doi/10.1002/2017GL074304.

O'Neill, B. C., and Coauthors, 2016: The scenario model intercomparison project (scenariomip) for cmip6. *Geoscientific Model Development*, **9**, 3461–3482, doi:10.5194/gmd-9-3461-2016.

Ouyang, Z., and Coauthors, 2020: Sea-ice loss amplifies summertime decadal co2 increase in the western arctic ocean. *Nature Climate Change*, **10**, 678–684, doi:10.1038/s41558-020-0784-2.

Petty, A. A., N. T. Kurtz, R. Kwok, T. Markus, and T. A. Neumann, 2020: Winter arctic sea ice thickness from icesat-2 freeboards. *Journal of Geophysical Research: Oceans*, **125**, doi:10.1029/2019JC015764.

Polyakov, I. V., and Coauthors, 2004: Variability of the intermediate atlantic water of the arctic ocean over the last 100 years. *Journal of Climate*, **17**, 4485–4497, doi:doi.org/10.1175/JCLI-3224.1, URL https://doi.org/10.1175/JCLI-3224.1.

Schlichtholz, P., 2011: Influence of oceanic heat variability on sea ice anomalies in the nordic seas. *Geophysical Research Letters*, **38**, doi:10.1029/2010GL045894.

Serreze, M. C., and W. N. Meier, 2019: The arctic's sea ice cover: trends, variability, predictability, and comparisons to the antarctic. *Annals of the New York Academy of Sciences*, **1436**, 36–53, doi:10.1111/NYAS.13856, URL https://onlinelibrary.wiley.com/doi/full/10.1111/nyas.13856https://onlinelibrary.wiley.com/doi/abs/10.1111/nyas.13856https://nyaspubs.onlinelibrary.wiley.com/doi/10.1111/nyas.13856.

Shim, S., Y.-J. Lim, Y.-H. Byun, J. Seo, S. Kwon, and B.-H. Kim, 2020: Nims-kma ukesm1.0-ll model output prepared for cmip6 cmip. Earth System Grid Federation, URL https://doi.org/10.22033/ESGF/CMIP6.2245, doi:10.22033/ESGF/CMIP6.2245.

Steele, M., and T. Boyd, 1998: Retreat of the cold halocline layer in the arctic ocean. *Journal of Geophysical Research: Oceans*, **103**, 10 419–10 435, doi:10.1029/98jc00580.

Stroeve, J., and D. Notz, 2018: Changing state of arctic sea ice across all seasons. Institute of Physics Publishing, doi:10.1088/1748-9326/aade56.

Sumata, H., L. de Steur, D. V. Divine, M. A. Granskog, and S. Gerland, 2023: Regime shift in arctic ocean sea ice thickness. *Nature*, **615**, 443–449, doi:10.1038/s41586-022-05686-x.

Swart, N. C., and Coauthors, 2019: The canadian earth system model version 5 (canesm5.0.3). *Geoscientific Model Development*, **12**, 4823–4873, doi:10.5194/gmd-12-4823-2019.

Vihma, T., 2014: Effects of arctic sea ice decline on weather and climate: A review. *Surveys in Geophysics*, **35**, 1175–1214, doi:10.1007/s10712-014-9284-0.

Voldoire, A., and Coauthors, 2019: Evaluation of cmip6 deck experiments with cnrm-cm6-1. *Journal of Advances in Modeling Earth Systems*, **11**, 2177–2213, doi:10.1029/2019MS001683, URL https://onlinelibrary.wiley.com/doi/full/10.1029/2019MS001683https://onlinelibrary.wiley.com/doi/abs/10.1029/2019MS001683https://agupubs.onlinelibrary.wiley.com/doi/10.1029/2019MS001683.

Winton, M., 2003: On the climatic impact of ocean circulation. URL http://www.cgd.ucar.edu/cas/catalog.

Årthun, M., T. Eldevik, L. H. Smedsrud, Skagseth, and R. B. Ingvaldsen, 2012: Quantifying the influence of atlantic heat on barents sea ice variability and retreat. *Journal of Climate*, **25**, 4736–4743, doi:10.1175/JCLI-D-11-00466.1, URL https://journals.ametsoc.org/view/journals/clim/25/13/jcli-d-11-00466.1.xml.